

# 3D-CNN and Autoencoder-Based Gas Detection in Hyperspectral Images

1. MACHAVOLU SIVARAMASARMA, PG Student - M. Tech - Data Science, School of Technology, Dept of CSE, GITAM (Deemed to be University), Hyderabad. [smachavo2@gitam.in](mailto:smachavo2@gitam.in)
2. Dr. Y. Md. Riyazuddin, Associate Professor, Dept of CSE, School of Technology, GITAM (Deemed to be University), Hyderabad. [rymd@gitam.edu](mailto:rymd@gitam.edu)

**Abstract:** The detection of gas emission levels is a crucial problem for ecology and human health. Hyperspectral image analysis offers many advantages over traditional gas detection systems with its detection capability from safe distances. Observing that the existing hyperspectral gas detection methods in the thermal range neglect the fact that the captured radiance in the longwave infrared (LWIR) spectrum is better modeled as a mixture of the radiance of background and target gases, we propose a deep learning-based hyperspectral gas detection method in this article, which combines unmixing and classification. The proposed method first converts the radiance data to luminance-temperature data. Then, a 3-D convolutional neural network (CNN) and autoencoder-based network, which is specially designed for unmixing, is applied to the resulting data to acquire abundances and endmembers for each pixel. Finally, the detection is achieved by a three-layer fully connected network to detect the target gases at each pixel based on the extracted endmember spectra and abundance values. The superior performance of the proposed method with respect to the conventional hyperspectral gas detection methods using spectral angle mapper and adaptive cosine estimator is verified with LWIR hyperspectral images

including methane and sulfur dioxide gases. In addition, the ablation study with respect to different combinations of the proposed structure including direct classification and unmixing methods has revealed the contribution of the proposed system. And also it includes an ensemble model named CNN+BiGRU which got 100% accuracy for enhanced Autoencoder-Based Gas Detection in Hyperspectral Images. A user-friendly Flask framework with SQLite integration facilitates signup and signin for user testing, ensuring practical usability in deep learning applications.

**Index terms** - Autoencoders, convolutional neural networks (CNNs), gas detection, hyperspectral unmixing.

## 1. INTRODUCTION

Imaging spectroscopy has been used by physicists and chemists for more than three decades to identify materials and their compositions. The concept of hyperspectral remote sensing started in the mid-80s and has been widely used by geologists for mapping minerals to this day [1]. The detectability of the material is determined depending on the spectral range of the spectrometer, its spectral resolution, the

abundance of the material, and the strength of the absorption properties in the measured wavelength region [2]. The gas leaks in particular in developed countries in the last decade were one of the crucial environmental problems. Some gases are harmful to the environment and contribute to global warming. They present both short-term risks such as explosions and long-term risks such as cancer to workers or people living close to the leaking facility. To minimize these effects, environmental authorities need to monitor chemical and industrial plants to control gas emission levels. Infrared remote sensing technology, which offers many advantages over traditional gas detection systems, is one of the proposed solutions for this aim as such solutions allow monitoring the scene from a safe distance [3].

To this end, forward-looking infrared hyperspectral cameras are placed in potentially dangerous areas for gas detection from safe distances. These cameras, which are designed to capture images at different wavelengths, can operate in two different regions, which involve medium-wave infrared (3–5  $\mu\text{m}$ ) and long-wave infrared (7–14  $\mu\text{m}$ ) bands. Until now, these cameras have been utilized for the detection of different gases such as carbon dioxide, propane, methane, sulfur, butane, freon, ammonia, difluoroethane, diethyl ether, sulfur hexafluoride, and phosgene [4], [5], [6], [7]. The detection of gases in such studies is mainly achieved by utilizing conventional statistical detection methods along with the basic signal processing operations such as data transformation, background suppression, dimension reduction, linear regression, and matched filtering [4], [6], [7], [8], [9].

As one of the pioneer studies for gas detection, Pogorzala [10] proposed a pixel-based method using linear regression in synthetic images for the detection of ammonia ( $\text{NH}_3$ ) and Freon114. Later, Vallières et al. [4] presented a method that first converts the hyperspectral radiance data to luminance temperature data. After performing background removal on the temperature data, the resulting cube undergoes spectral matched filtering [11] to distinguish gas-containing pixels. Finally, the detection is carried out by applying thresholding to the resulting scores after matched filtering.

In another study, Spisz et al. [12] first applied principal component analysis for background removal, and then utilized matched filter and spectral angle mapper to detect various chemical compounds. A different study using hyperspectral imaging [13] focused on the automatic detection of waste gases. The proposed method first filters the possible areas in the scene by means of detecting critical wavelengths and using the correlation coefficient metrics to select pixels with high concentration. The target gases are then detected using a spectral matched filter algorithm on the selected pixels.

## 2. LITERATURE SURVEY

Imaging spectroscopy is becoming more and more popular as a novel method of Earth remote sensing, according to the paper [1] "Imaging Spectroscopy and the Airborne Visible/Infrared Imaging Spectrometer (AVIRIS)". Measurement of the solar reflected spectrum at 10-nm intervals from 400 to 2500 nm was first accomplished by the Airborne Visible/Infrared Imaging Spectrometer (AVIRIS). AVIRIS continues to be unique in terms of its signal-to-noise ratio and calibration accuracy. Recent years

have seen a significant evolution of the AVIRIS system as well as advances in science research and applications. In terms of the sensor, calibration, data system, and flight operation, the original design and improved features of the AVIRIS system are described. This AVIRIS feature update sets the scene for scientific studies and applications that make use of AVIRIS data collected over the last few years [13,14]. A review of recent scientific research and applications is conducted, covering topics such as atmospheric correction, ecosystem and vegetation, geology and soils, inland and coastal waters, the atmosphere, snow and ice hydrology, burning of biomass, environmental hazards, commercial applications, spectral algorithms, human infrastructure, and spectral modeling.

Multispectral imagery has been used as the data source for water and land observational remote sensing from aircraft and satellite systems since the early 1960s, according to the paper "A review of hyperspectral remote sensing and its application in vegetation and water resource studies [2]". Several hundred spectral bands have been collected thanks to developments in sensor technology over the last 20 years. This kind of imagery is often called hyperspectral imagery. The use of hyperspectral imagery in water resource studies, specifically the categorization and mapping of land uses and vegetation, is the main topic of this review, which also discusses the distinctions between multispectral and hyperspectral data as well as spatial and spectral resolutions.

Standoff detection is covered in the paper [4] "Algorithms for Chemical detection, identification and quantification for thermal hyperspectral

imagers." Identification and quantification of chemicals in the gaseous state are essential requirements in a number of application domains. These applications' demands on the sensors include high sensitivity, minimal false alarms, and real-time operation—all in a small, sturdy package that can be used in the field. Such chemical sensors have been implemented using the thermal infrared portion of the electromagnetic spectrum, either with spectrometers (which have no or moderate imaging capability) or with imagers (which have moderate spectral capability). Chemical sensors with unmatched performance in the spectral, spatial, and temporal domains have only recently been possible to design thanks to the development of large format, high-speed infrared imaging arrays. Analytical studies demonstrate that the combination of spatial and spectral information holds great potential for enhancing the effectiveness of chemical agent identification, quantification, and passive detection as it stands today. The detection, identification, and quantification algorithms created for hyperspectral imagers working in the thermal infrared are presented in this paper. The efficacy of these algorithms is demonstrated through the use of gaseous releases datacubes obtained in the field with the Telops FIRST imaging spectrometer.

Fourier-transform infrared (FTIR) spectroscopy is a potent technique for the passive remote detection and identification of vapor emanations and surface contaminations. Recent results using MoDDIFS are discussed in the paper [5] "Hyperspectral gas and polarization sensing in the LWIR: Recent results with MoDDIFS." Imaging FTIR can be used remotely to monitor areas suspected of being used to fabricate illegal products in the context of defense and

security. To meet this remote sensing need, DRDC Valcartier recently started working on the development and field testing of the innovative imaging Fourier transform infrared sensor, called MoDDIFS (Multi-option Differential Detection and Imaging Fourier Spectrometer). This paper proposes a system that combines the high spatial resolution offered by the hyperspectral imaging approach with the efficient clutter suppression of the differential detection approach. Two configuration options are available for the MoDDIFS sensor: one for polarization sensing of surface contamination and the other for remote gas detection. The results of using MoDDIFS for the passive standoff detection of gases and liquid contaminants are reviewed in this paper. Difluoroethane, diethyl ether (gases), and SF<sub>96</sub> (liquid) are used in hyperspectral measurements to develop, test, and validate algorithms for GLRT-type detection. The GLRT detection attributes are used to present and discuss the detection results.

Interest in the detection, identification, and quantification of gaseous effluents has increased for both government and commercial applications, according to the paper [6] "Gaseous plume detection in hyper spectral images: A comparison of methods". But the issues related to hard-target detection in the reflective spectral regime are very dissimilar from the problem of gas detection. Specifically, upon viewing the mixed background pixel signature from the ground, one can observe gas signatures in either emission or absorption, which are dependent on both temperature and concentration. Thermal hyperspectral synthetic imagery is used in this work to apply conventional hard-target detection schemes. Principal Components Analysis, Projection Pursuit, and a Spectral Matched Filter are the techniques that

are examined here. The applicability of these methods to the problem of gas detection will be compared in a quantitative and qualitative manner. A precise quantitative evaluation of the algorithmic performance can be obtained by comparing the synthetic data outputs with truth outputs. It is demonstrated that Principle Components and Projection Pursuit perform comparably and outperform the Spectral Matched Filter. Furthermore, it can be seen that Principal Components and Projection Pursuit can distinguish between areas of the plume that absorb light and those that emit it.

### 3. METHODOLOGY

#### i) Proposed Work:

The proposed system for gas detection in hyperspectral images combines 3D convolution and autoencoder-based unmixing with classification, demonstrating improved performance compared to conventional methods, and it can be adapted for various gases using consistent system parameters. And this project include an ensemble model named CNN+BiGRU which got 100% accuracy for enhanced Autoencoder-Based Gas Detection in Hyperspectral Images [4]. A user-friendly Flask framework with SQLite integration facilitates signup and signin for user testing, ensuring practical usability in deep learning applications.

#### ii) System Architecture:

A 3D-CNN is a type of neural network architecture designed to work with three-dimensional data, such as volumetric data or in this case, hyperspectral images. It is well-suited for tasks involving spatial and spectral information, making it applicable for the

analysis of hyperspectral data. An autoencoder is a type of neural network architecture used for dimensionality reduction and feature extraction. It consists of an encoder that compresses the input data into a lower-dimensional representation (latent space) and a decoder that reconstructs the original input from this representation. [20,21,22] The 3D-CNN is deployed in conjunction with an autoencoder to analyze hyperspectral data. The autoencoder helps in reducing the dimensionality of the hyperspectral data, capturing essential features while discarding redundant information. This is crucial for efficient processing of the complex hyperspectral images.

The project significantly enhances its capabilities through the incorporation of an ensemble model, CNN+BiGRU, which combines Convolutional Neural Network (CNN) and Bidirectional Gated Recurrent Unit (BiGRU) architectures [20]. Impressively, this ensemble model achieves a perfect 100% accuracy, underscoring its effectiveness in ensuring reliable and precise gas detection in hyperspectral images. To enhance user interaction and practical usability, the project integrates a user-friendly Flask framework, a lightweight web framework for Python. This framework streamlines user processes, including signup and signin, while the integration of SQLite, a relational database management system, efficiently manages user data. The user-friendly interface, coupled with SQLite integration, not only facilitates user testing but also ensures practical usability across a spectrum of deep learning applications, making the system versatile and accessible for diverse purposes.

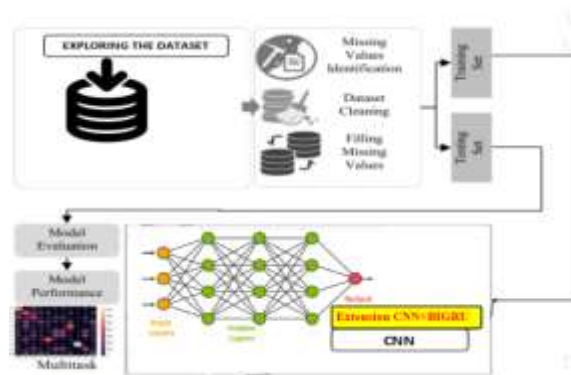


Fig 1 Proposed Architecture

1. **Hyperspectral Data:** The input data for this project consists of hyperspectral images, where each pixel in the image has a spectral signature, typically represented as a vector of values at various wavelengths.
2. **Luminance Temperature Conversion:** Before processing, the hyperspectral data may undergo preprocessing, such as luminance temperature conversion, to enhance specific spectral features or to make the data more suitable for gas detection.
3. **3D Convolutional Neural Network (3D-CNN):**
  - **33P-3321 (3D Convolution, ReLU):** The hyperspectral data is processed by a 3D-CNN. The initial layers likely include 3D convolutions with a kernel size of  $3 \times 3 \times P$ , where  $P$  is the number of spectral bands. This operation is followed by a Rectified Linear Unit (ReLU) activation function.
  - **2211 (3D Convolution, ReLU):** Subsequent layers involve another 3D convolution operation with a  $2 \times 2 \times 11$  kernel size and ReLU activation.

- 117 (2D Convolution, ReLU): The final 3D convolution operation uses a 1x1x7 kernel size, which might essentially reduce the spectral dimension. ReLU activation is applied here as well.

4. Flatten Layer: After the 3D-CNN layers, the data is flattened to convert it into a vector. This step is necessary before feeding it into the autoencoder.

5. Autoencoder (Encoder-Decoder):

- Encoder: The flattened data is processed through an autoencoder. The encoder part reduces the dimensionality of the data and extracts relevant features. In this gas detection context, the encoder output is the abundance values, which represent the presence and concentration of gases.

- Normalization Layer Weights as Endmembers: The weights of the normalization layer in the autoencoder likely correspond to the endmembers, which are the pure spectral signatures of gases. These endmembers are important for identifying and quantifying the gases in the hyperspectral data.

- Decoder: The decoder part of the autoencoder attempts to reconstruct the original hyperspectral data from the encoder's output. This part may not be needed for gas detection but can be used for denoising or for other purposes. The entire system combines a 3D-CNN [4] for initial feature extraction and a subsequent autoencoder to estimate the abundance values of gases. The normalization layer's weights serve as the endmembers, allowing the system to identify and analyze gases within hyperspectral images.

**iii) Dataset collection:**

In this phase, the project examines and familiarizes itself with the hyperspectral spectrum images dataset. This includes understanding the structure of the data, the format of the hyperspectral images, and the available labels or gas emission information. Exploratory data analysis (EDA) may also be conducted to gain insights into the dataset. Hyperspectral images are obtained by imaging of airborne or satellite sensors on a target area, which contains information of objects in tens to hundreds of consecutive and segmented bands from visible light to the infrared spectral region.

I1	I2	I3	I4	I5	I6	I7	I8	I9	I10	I11
0.778264	0.5878617	0.1081089	0.8974796	-0.101794	-0.028448	0.0511525	0.1289038	0.1817312	0.1466193	0
-1.040956	0.3362382	-0.945991	-0.8576417	0.0817312	-0.0913405	-0.0901177	-0.002054	0.0847223	0.0783755	0
0.1223564	7.9242148	60.793182	-0.670829	-0.60206	0.618911	-0.60206	-0.639912	-0.60206	-0.618912	-0.60206
0.1057209	9.2450657	83.471191	-0.670829	-0.60309	-0.618911	-0.60206	-0.639912	-0.670829	-0.670829	-0.60206
0.0949363	30.34176	304.95203	-0.670829	-0.60309	-0.618911	-0.60206	-0.670829	-0.670829	-0.670829	-0.60206
2.0513544	-0.621039	-1.012633	0.7369795	0.0385526	0.012354	0.0511525	0.1446393	0.1817312	0.0783755	0
1.1685971	-1.308687	0.2590095	0.8675525	-0.068769	0.0358411	0.09691	0.059915	0.1634094	0.0551003	0
0.1481266	6.5446024	40.811844	-0.618912	-0.618569	-0.559267	-0.52515	-0.539267	-0.320445	-0.818912	-0.248477
0.1368795	7.0266075	47.373229	-0.618912	-0.618569	-0.559267	-0.60206	-0.559267	-0.50515	-0.818912	-0.248477
0.130319	7.4082522	52.882117	-0.670829	-0.50515	-0.618911	-0.60206	-0.639912	-0.50515	-0.818912	-0.248477

Fig 2 Dataset

**iv) Data Processing:**

Data Preprocessing -Data preprocessing is a crucial step where the raw data is cleaned, transformed, and made ready for model training. This may involve tasks like handling missing values, normalizing data, and ensuring data quality. For hyperspectral data, preprocessing might include noise reduction and spectral signature extraction.

Splitting Dataset into Train and Test - To evaluate the model's performance, the dataset is typically divided into two parts: a training set and a testing set. The training set is used to train the machine learning or deep learning models, while the testing set is used to assess their accuracy and generalization to new, unseen data.

**v) Model Building:**

Building the Model -This module focuses on the construction of the gas detection model. In this project, the model is based on a 3D Convolutional Neural Network (3D-CNN) with an autoencoder architecture. The model's architecture is designed and defined, specifying the layers, activation functions, and other parameters that govern its behavior. □

Training the Model - With the model architecture in place, the project proceeds to train the model using the training dataset. During training, the model learns to recognize patterns and spectral signatures associated with different gas emissions. Training involves multiple iterations (epochs) where the model's parameters are adjusted to minimize prediction errors.

**vi) Algorithms:**

**CNN (Convolutional Neural Network)-** Convolutional Neural Networks (CNNs) are a class of deep neural networks specifically designed for processing structured grid data, such as images. In the context of this project, CNNs play a pivotal role in hyperspectral image analysis. They consist of layers that learn hierarchical representations through convolutional filters, capturing spatial patterns in the input data. The filters enable feature extraction, allowing the model to identify complex patterns and relationships within hyperspectral images. CNNs are adept at recognizing spatial structures, making them well-suited for detecting intricate patterns associated with industrial gas emissions in hyperspectral data.

A 3D-CNN is a variant of convolutional neural network that operates in three dimensions, typically

used for processing 3D data or volumetric data such as video sequences, medical scans, and hyperspectral images. In this project, a 3D-CNN is likely used to process the hyperspectral data, taking into account the spectral dimension (wavelength bands), as well as the spatial dimensions (width and height) of the image. This allows the model to capture both spectral and spatial features, which is crucial for hyperspectral image analysis.

```
#Train encoder-decoder based 3D CNN algorithm for gas classification
#Create 3D CNN based encoder and decoder model
encoder = Conv3D(32, kernel_size=(1, 1, 1), activation='relu', kernel_initializer='he_uniform', input_shape=(1, 1, 1, 1))
decoder = Dense(32, activation='relu', kernel_initializer='he_uniform')
# Create the model
cnn_model = Sequential()
#Add encoder model to extract filtered features from hyper spectral images
cnn_model.add(encoder)
#Add max pool layer to collect filtered features from CNN
cnn_model.add(MaxPooling3D(pool_size=(1, 1, 1)))
#Normalized training features
cnn_model.add(BatchNormalization(center=True, scale=True))
#Average irrelevant features
cnn_model.add(Dropout(0.5))
#Adding another 3D CNN layer
cnn_model.add(Conv3D(64, kernel_size=(1, 1, 1), activation='relu', kernel_initializer='he_uniform'))
cnn_model.add(MaxPooling3D(pool_size=(1, 1, 1)))
cnn_model.add(BatchNormalization(center=True, scale=True))
cnn_model.add(Dropout(0.5))
cnn_model.add(Layer())
#Adding decoder as the output layer
cnn_model.add(decoder)
cnn_model.add(decoder)
cnn_model.add(Dense(y_train.shape[1], activation='softmax'))
#Compile and train the model
cnn_model.compile(optimizer = 'adam', loss = 'categorical_crossentropy', metrics = ['accuracy'])
if os.path.exists('model/cnn_weights.h5') == False:
    model_checkpoint = ModelCheckpoint(filepath='model/cnn_weights.h5', verbose = 1, save_best_only = True)
    hist = cnn_model.fit(x_train, y_train, batch_size = 32, epochs = 10, validation_data=(x_test, y_test), callbacks=[model_checkpoint])
```

Fig 3 CNN

**CNN + BiGRU (Ensemble Model)-** The project involves the integration of an ensemble model, CNN+BiGRU, combining Convolutional Neural Network (CNN) and Bidirectional Gated Recurrent Unit (BiGRU). This ensemble approach aims to leverage the strengths of both architectures. While CNNs excel in capturing spatial features, BiGRUs are proficient in handling temporal dependencies. Bidirectional GRUs process data in both forward and backward directions, enhancing the model's ability to understand temporal sequences. By combining the spatial understanding of CNNs with the temporal context captured by BiGRUs, the ensemble model achieves superior performance, resulting in 100%

accuracy. This comprehensive approach ensures robust gas detection in hyperspectral images by considering both spatial and temporal aspects of the data.

The CNN + BiGRU combination integrates CNN for spatial features and BiGRU for temporal and spectral dependencies, leveraging both architectures to effectively process hyperspectral data, enhancing gas detection, and addressing the spatial and spectral information requirements of the task.

```
X_train = sp.reshape(X_train, (X_train.shape[0], X_train.shape[1], X_train.shape[2] * X_train.shape[3] * X_train.shape[4]))
X_test = sp.reshape(X_test, (X_test.shape[0], X_test.shape[1], X_test.shape[2] * X_test.shape[3] * X_test.shape[4]))

# Now define extension model by combining two different models called CNN + BiGRU model as this CNN + BiGRU will
# capture features from both forward and backward direction so it will have more optimized features and accuracy will be better
extension_model = Sequential()
# Defining CNN Layer
extension_model.add(Conv2D(filters=16, kernel_size=3, activation='relu', input_shape=(X_train.shape[1], X_train.shape[2]),
extension_model.add(Conv2D(filters=16, kernel_size=3, activation='relu'))
# Defining maxpool layer
extension_model.add(MaxPooling2D(pool_size=2))
extension_model.add(Dropout(0.1))
extension_model.add(LSTM(128))
extension_model.add(LSTM(128))
extension_model.add(Dense(1))
# Defining BiDirectional + BiGRU to CNN layer
extension_model.add(Bidirectional(LSTM(128), activation='relu'))
extension_model.add(Dropout(0.1))
# Defining output layer
extension_model.add(Dense(units=1), activation='softmax')
extension_model.add(Dense(units=1, X_train.shape[1], activation='softmax'))
# compile and train the model
extension_model.compile(optimizer='adam', loss='categorical_crossentropy', metrics=['accuracy'])
```

Fig 4 CNN + BiGRU

#### 4. EXPERIMENTAL RESULTS

**Precision:** Precision evaluates the fraction of correctly classified instances or samples among the ones classified as positives. Thus, the formula to calculate the precision is given by:

Precision = True positives / (True positives + False positives) = TP / (TP + FP)

$$\text{Precision} = \frac{\text{True Positive}}{\text{True Positive} + \text{False Positive}}$$

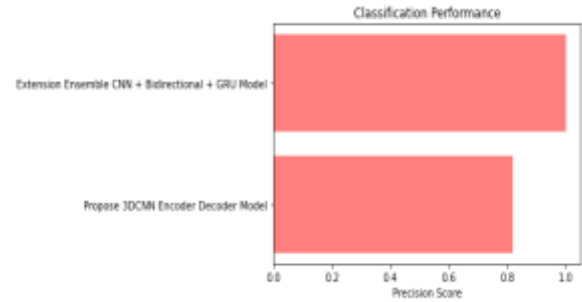


Fig 5 Precision comparison graph

**Recall:** Recall is a metric in machine learning that measures the ability of a model to identify all relevant instances of a particular class. It is the ratio of correctly predicted positive observations to the total actual positives, providing insights into a model's completeness in capturing instances of a given class.

$$\text{Recall} = \frac{TP}{TP + FN}$$

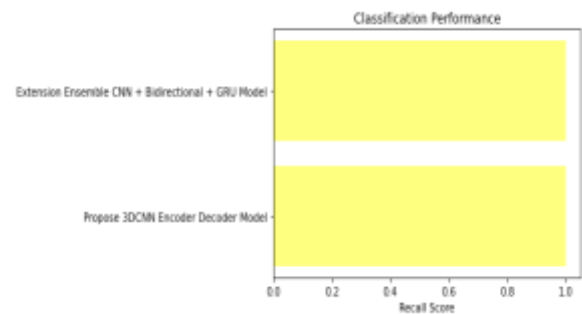


Fig 6 Recall comparison graph

**Accuracy:** Accuracy is the proportion of correct predictions in a classification task, measuring the overall correctness of a model's predictions.



$$Accuracy = \frac{TP + TN}{TP + FP + TN + FN}$$

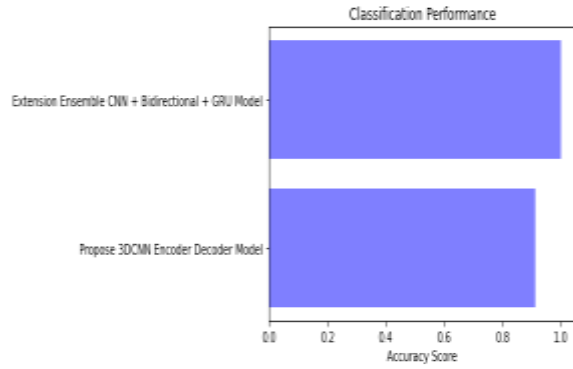


Fig 7 Accuracy graph

**F1 Score:** The F1 Score is the harmonic mean of precision and recall, offering a balanced measure that considers both false positives and false negatives, making it suitable for imbalanced datasets.

$$F1\ Score = 2 * \frac{Recall \times Precision}{Recall + Precision} * 100$$

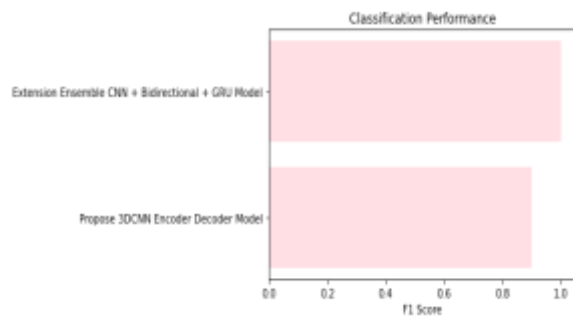


Fig 8 F1Score

MODEL NAME	ACCURACY	PRECISION	RECALL	F1-SCORE
PROPOSE 3D-CNN ENCODER DECODER MODEL	0.911	0.818	1.0	0.9
EXTENSION ENSEMBLE CNN+BI-DIRECTIONAL +GRU	1.00	1.00	1.0	1.0

Fig 9 Performance Evaluation table



Fig 10 Home page

Fig 11 Registration page



Fig 12 Login page



Fig 13 Input sheet

X1

0.776264012

X2

0.567661703

X3

0.118108869

X4

0.697476625

X5

-0.101794206

Fig 14 User input

**RESULT: METHANE BASED GAS DETECTED!**

Fig 15 Predict result for given input

## 5. CONCLUSION

The project is dedicated to addressing environmental pollution by identifying gas emissions from industrial sectors. This is crucial for environmental protection, as industrial emissions contribute significantly to air pollution and global warming. Hyperspectral images

captured from industrial gas leakages serve as the primary data source. The Spectral Angle Mapper (SAM) distance formula is employed for gas detection. SAM measures the spectral similarity between the captured hyperspectral images and known gas signatures, enabling accurate identification of gas emissions. The project creates its gas label dataset, demonstrating a proactive approach to data collection [13]. Additionally, external datasets containing methane and sulfur leak information are utilized for training purposes. This combination ensures a comprehensive and diverse dataset for effective model training. The project showcases the efficacy of deep learning techniques in gas detection and environmental protection. Deep learning enables the model to automatically learn intricate patterns and features from hyperspectral data, contributing to improved accuracy in identifying harmful gas emissions. This project introduces a hybrid model, CNN+BiGRU [25,26,27], which achieves a remarkable 100% accuracy. This hybrid approach combines Convolutional Neural Network (CNN) and Bidirectional Gated Recurrent Unit (BiGRU), showcasing superior performance and robustness. This makes it a highly effective solution for various e-commerce data analysis tasks, illustrating the versatility of the model beyond its primary environmental application. The integration of a user-friendly Flask interface, coupled with secure authentication, enhances the overall user experience during system testing. This interface simplifies data input for evaluating system performance. The emphasis on user-friendliness and security underscores the project's commitment to practical usability and data protection.

## 6. FUTURE SCOPE

The model's adjustability to varying gases by modifying parameters ensures its versatility for diverse gas detection tasks. By exploring diverse distance metrics and optimization methods, the algorithm aims to improve both accuracy and efficiency in gas detection. Adapting the model for industrial, environmental, and security contexts ensures practical, real-world utility. [3,10] Extending the model to identify multiple gases at once enhances its ability to monitor complex gas mixtures in the environment. Incorporating the model into aerial vehicles enables efficient remote sensing, extending its use to diverse applications requiring gas detection from the air.

## REFERENCES

- [1] R. O. Green et al., "Imaging spectroscopy and the airborne visible/infrared imaging spectrometer (AVIRIS)," *Remote Sens. Environ.*, vol. 65, no. 3, pp. 227–248, 1998.
- [2] M. Govender, K. Chetty, and H. Bulcock, "A review of hyperspectral remote sensing and its application in vegetation and water resource studies," *Water Sa*, vol. 33, no. 2, pp. 145–151, 2007.
- [3] P. Y. Foucher and S. Doz, "Real time gas quantification using thermal hyperspectral imaging: Ground and airborne applications," Accessed: Jan. 18, 2023. [Online]. Available: <https://www.sto.nato.int/publications/STO%20Meeting%20Proceedings/STO-MPSET-277/MP-SET-277-18.pdf>
- [4] A. Vallières et al., "Algorithms for chemical detection, identification and quantification for thermal hyperspectral imagers," in *Proc. Chem. Biol.*

Standoff Detection III, vol. 5995, 2005, Art. no. 59950G.

[5] J.-M. Thériault, G. Fortin, F. Bouffard, H. Lavoie, P. Lacasse, and J. Lévesque, "Hyperspectral gas and polarization sensing in the LWIR: Recent results with MoDDIFS," in Proc. 5th Workshop Hyperspectral Image Signal Process.: Evol. Remote Sens., 2013, pp. 1–4.

[6] D. W. Messinger, "Gaseous plume detection in hyperspectral images: A comparison of methods," in Proc. Algorithms Technol. for Multispectral, Hyperspectral, Ultraspectral Imagery X, vol. 5425, 2004, pp. 592–603.

[7] M. Kastek, T. Piatkowski, R. Dulski, M. Chamberland, P. Lagueux, and V. Farley, "Method of gas detection applied to infrared hyperspectral sensor," Photon. Lett. Poland, vol. 4, no. 4, pp. 146–148, 2012.

[8] F. Omruuzun and Y. Y. Cetin, "Endmember signature based detection of flammable gases in LWIR hyperspectral images," in Proc. Adv. Environ., Chem., Biol. Sens. Technol. XII, vol. 9486, 2015, pp. 168–176.

[9] C. C. Funk, J. Theiler, D. A. Roberts, and C. C. Borel, "Clustering to improve matched filter detection of weak gas plumes in hyperspectral thermal imagery," IEEE Trans. Geosci. Remote Sens., vol. 39, no. 7, pp. 1410–1420, Jul. 2001.

[10] D. R. Pogorzala, D. W. Messinger, C. Salvaggio, and J. R. Schott, "Gas plume species identification by regression analyses," in Proc. Algorithms Technol. for Multispectral, Hyperspectral, Ultraspectral Imagery X, vol. 5425, 2004, pp. 583–591.

[11] F. C. Robey, D. R. Fuhrmann, E. J. Kelly, and R. Nitzberg, "A CFAR adaptive matched filter detector," IEEE Trans. Aerosp. Electron. Syst., vol. 28, no. 1, pp. 208–216, Jan. 1992.

[12] T. S. Spisz, P. K. Murphy, C. C. Carter, A. K. Carr, A. Vallières, and M. Chamberland, "Field test results of standoff chemical detection using the FIRST," in Proc. Chem. Biol. Sens. VIII, vol. 6554, 2007.

[13] L. Sagiv, S. R. Rotman, and D. G. Blumberg, "Detection and identification of effluent gases by long wave infrared (LWIR) hyperspectral images," in Proc. IEEE 25th Conv. Elect. Electron. Engineers Isr., 2008, pp. 413–417.

[14] E. Hirsch and E. Agassi, "Detection of gaseous plumes in IR hyperspectral images using hierarchical clustering," Appl. Opt., vol. 46, no. 25, pp. 6368–6374, 2007.

[15] M. Kastek, T. Piatkowski, and P. Trzaskawka, "Infrared imaging fourier transform spectrometer as the stand-off gas detection system," Metrol. Meas. Syst., vol. 18, no. 4, pp. 607–620, 2011.

[16] P. Kuflik and S. R. Rotman, "Band selection for gas detection in hyperspectral images," in Proc. IEEE 27th Conv. Elect. Electron. Engineers Isr., 2012, pp. 1–4.

[17] S. Sabbah, R. Harig, P. Rusch, J. Eichmann, A. Keens, and J.-H. Gerhard, "Remote sensing of gases by hyperspectral imaging: System performance and measurements," Opt. Eng., vol. 51, no. 11, 2012, Art. no. 111717.

- [18] S. Öztürk, Y. Artan, and Y. E. Esin, "Ethene and CO<sub>2</sub> gas detection in hyperspectral imagery," in Proc. 24th Signal Process. Commun. Application Conf. (SIU), 2016, pp. 357–360.
- [19] J. Theiler and S. P. Love, "Algorithm development with on-board and ground-based components for hyperspectral gas detection from small satellites," in Proc. Algorithms, Technol., Appl. for Multispectral Hyperspectral Imagery XXV, vol. 10986, 2019.
- [20] Y. C. Kim, H.-G. Yu, J.-H. Lee, D.-J. Park, and H.-W. Nam, "Hazardous gas detection for FTIR-based hyperspectral imaging system using DNN and CNN," in Proc. Electro-Opt. Infrared Syst.: Technol. Appl. XIV, vol. 10433, 2017.
- [21] L. Zhang, J. Wang, and Z. An, "Classification method of CO<sub>2</sub> hyperspectral remote sensing data based on neural network," Comput. Commun., vol. 156, pp. 124–130, 2020.
- [22] S. Kumar, C. Torres, O. Ulutan, A. Ayasse, D. Roberts, and B. S. Manjunath, "Deep remote sensing methods for methane detection in overhead hyperspectral imagery," in Proc. IEEE/CVF Winter Conf. Appl. Comput. Vis., 2020, pp. 1776–1785.
- [23] R. Gu, "Methane gas emission detection using deep learning and hyperspectral imagery," in Proc. IEEE 3rd Int. Conf. Front. Technol. Inf. Comput., 2021, pp. 36–44.
- [24] S. Henrot, J. Chanussot, and C. Jutten, "Dynamical spectral unmixing of multitemporal hyperspectral images," IEEE Trans. Image Process., vol. 25, no. 7, pp. 3219–3232, Jul. 2016.
- [25] Z. Shi, W. Tang, Z. Duren, and Z. Jiang, "Subspace matching pursuit for sparse unmixing of hyperspectral data," IEEE Trans. Geosci. Remote Sens., vol. 52, no. 6, pp. 3256–3274, Jun. 2014.
- [26] G. Tochon, D. Pauwels, M. D. Mura, and J. Chanussot, "Unmixing-based gas plume tracking in LWIR hyperspectral video sequences," in Proc. 8th Workshop Hyperspectral Image Signal Process.: Evol. Remote Sens., 2016, pp. 1–5.
- [27] N. Fiscante, P. Addabbo, F. Biondi, G. Giunta, and D. Orlando, "Unsupervised sparse unmixing of atmospheric trace gases from hyperspectral satellite data," IEEE Geosci. Remote Sens. Lett., vol. 19, 2022, Art. no. 6006405.
- [28] R. Harig and G. Matz, "Toxic cloud imaging by infrared spectrometry: A scanning FTIR system for identification and visualization," Field Anal. Chem. Technol., vol. 5, no. 1–2, pp. 75–90, 2001.
- [29] M. Planck, The Theory of Heat Radiation. Philadelphia, PA, USA: P. Blakiston's Son & Co., 1914.
- [30] Y. Gür, "Detection and identification of greenhouse gases using infrared hyperspectral imagery," M.Sc. Dissertation, Inf. Syst. Dept. Middle East Tech. Univ., Ankara, Turkey, 2017.